# DEVELOPMENT OF A SUB-GRID LIQUID JET CONDENSATION MODEL

**F. X. Buschman and D. L. Aumiller**
Bettis Atomic Power Laboratory
West Mifflin, Pennsylvania, USA
Francis.Buschman@unnpp.gov

**ABSTRACT**

Condensation on liquid jets is an important phenomenon for many different facets of nuclear power plant transients and analyses such as containment spray cooling. The data obtained at the High Pressure Liquid Jet Condensation Heat Transfer facility (HPLJCHT), an experimental facility constructed at the Pennsylvania State University, have been used to develop constitutive relations describing direct contact condensation heat transfer on liquid jets, in pure steam and in the presence of noncondensable gas.

This paper describes a new sub-grid liquid jet condensation heat transfer model. In the current work, mass and energy balance equations are solved in a marching scheme in each sub-grid node along the path of the jet trajectory. Jet specific condensation heat transfer closure relations are used. The jet sub-grid method has been implemented as a boundary condition in an in-house version of the sub-channel analysis code COBRA-TF (COBRA-IE). COBRA-IE fluid nodes provide the required vapor and noncondensable gas conditions for the heat transfer solution. The sub-grid model solves the liquid side heat transfer and the condensation rates for each volume in the sub-grid solution. These terms are summed along all of the sub-grid cells that pass through each COBRA-IE control volume to provide mass and energy transfer rates for the COBRA-IE solution. Results using the new jet injection boundary condition show an improved ability to simulate jet condensation experimental data.

**KEYWORDS**
Jet Condensation, Sub-grid, Sub-channel, Noncondensable Gas

## 1. INTRODUCTION

Condensation on liquid jets is an important phenomenon for many different facets of nuclear power plant transients and analyses such as containment spray cooling. A new experimental facility constructed at the Pennsylvania State University, the HPLJCHT facility, has been used to perform steady-state condensation heat transfer experiments in which the temperature of the liquid jet is measured at different axial locations, allowing the condensation rate to be determined over the jet length. Test data have been obtained in a pure steam environment and with varying concentrations of noncondensable gas. The data taken at this facility represent the first high-pressure, jet condensation data that include noncondensable gases. The data have been used to develop constitutive relations describing direct contact condensation heat transfer on liquid jets, in pure steam and in the presence of noncondensable gas [1].

A new sub-grid liquid jet condensation heat transfer model, implemented as a specialized jet injection boundary condition, has been implemented in COBRA-IE in order to model the experiments performed at the HPLJCHT, hereafter referred to as the Fundamental Condensation Test. The jet injection boundary condition allows the use of jet specific condensation heat transfer closure relations using local conditions while solving mass and energy balance equations in a marching scheme along the jet length. The development and implementation of the jet injection boundary condition follows the methodology developed by Buschman [2].

## 2. JET INJECTION BOUNDARY CONDITION DEFINITION

Prior to the development of this model, accurate modeling of condensation on liquid jets in COBRA–IE was precluded due to assumptions made in physics implemented in the code [2]. Specifically, COBRA–IE assumes that any continuous liquid present is in the form of a film that adheres to the wetted perimeter of the sub-channel. The other available option would be to assume that the entirety of the jet is injected as droplets which would be assumed to be dispersed throughout the sub-channel. Both of these assumptions are incompatible with

the physical nature of a jet flowing through an open environment. To improve the code's ability to model jets, and specifically condensation on a liquid jet, a new jet injection boundary condition has been added.

The jet injection boundary condition solves conservation of mass and energy equations in a marching algorithm along the length of the jet on a sub-grid mesh. An example of a sub-grid mesh overlaid on a standard sub-channel mesh is given in Figure 1. In Figure 1, the COBRA–IE computational mesh is represented by the solid black lines. The jet conservation equations are solved on the finer mesh represented by the blue shaded region and dashed lines. Solving the jet conservation equations on the finer sub-grid provides a more detailed estimate of the condensation rate on the jet within the COBRA–IE node. The user inputs the jet path details, including which COBRA–IE nodes the jet passes through in order and the length of the jet within each node.

The jet injection boundary condition has been implemented in a way that provides flexibility to the user. The pressure at boundary condition location is used in the calculation of the total boundary condition flow rate. Multiple jet trajectories, called paths, can be input per boundary condition location. The physical trajectory of each path is input by specifying, in order, the COBRA-IE control volumes through which the jet passes as well as the length of the jet flow path within that volume. In this way the user can specify a jet trajectory that is not limited to a single sub-channel or axial section. For each jet path the following input is provided:

(a) Fraction of total boundary condition flow for an individual jet following this path,
(b) Number of actual jets which follow the same path,
(c) Number of COBRA-IE control volumes through which the path traverses,
(d) Number of path ends, and
(e) Jet diameter.

In order to conserve the volumetric flow rate calculated by the injection boundary condition balance equation, input for items (a) and (b) above should be such that when their product is summed over all the paths in a boundary condition the result is 1.0. For each COBRA-IE control volume in the path the user must input:

(a) COBRA-IE channel number ($I$),
(b) COBRA-IE axial level ($J$) within the channel, and
(c) Length of the jet in the COBRA-IE control volume.

The flexibility in the sub-grid jet model implementation provides a means for distributing the liquid associated with the jet at its end in a user defined manner. In this way, a user could account for a jet hitting a structure and fracturing with some of the liquid forming a film on the structure and the remainder forming droplets in a different location. This is done by specifying multiple jet ends for a single jet path. For each path end the following is input:

(a) COBRA-IE channel ($I$),
(b) COBRA-IE axial level ($J$),
(c) Fraction of path flow which goes to this end,
(d) Droplet size, and
(e) Fraction of end flow that is droplets.

In order to conserve mass, the user should ensure the sum of the product of the end fractions and Number of jets represented by the path is 1.0.

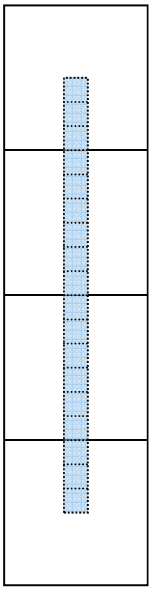

**Figure 1: Jet Injection Boundary Condition Sub-grid**

## 3. JET CLOSURE RELATIONS

Using the jet injection boundary conditions also allows the use of jet specific closure relations for the condensation heat transfer coefficient and for condensation suppression in the presence of a noncondensable gas. These closure relations, which are strong functions of local conditions within the jet, are then calculated on the fine mesh to provide a more accurate prediction of the local condensation rate. The correlation for the jet condensation heat transfer coefficient is developed in the process of analyzing the Fundamental Condensation Test data and is given as:

$$St(x) = 9.7\text{x}10^{-4}\left(\frac{x}{D_{jet}(x)}\right)^{-0.21} We(x)^{0.54}\left(\frac{\rho_l(x)}{\rho_g(x)}\right)^{-0.49} \quad (1)$$

where $St$ is the Stanton Number, $x$ is the distance from the beginning of the jet, $D_{jet}$ is the jet diameter, $We$ is the Weber Number, $\rho_l$ is the liquid density, and $\rho_g$ is the gas density. The Stanton Number, $St$, is a ratio of the Nusselt Number, $Nu$, and the product of the Reynolds Number, $Re$, and Prandtl Number, $Pr$:

$$St(x) = \frac{Nu(x)}{Re\ (x)Pr(x)} \quad (2)$$

The Weber Number, $We$, is a ratio of the jet inertial force to surface tension given as:

$$We(x) = \frac{\rho_l(x)U_{jet}^2 D_{jet}(x)}{\sigma} \quad (3)$$

where $U_{jet}$ is the local jet velocity and $D_{jet}$ is the jet diameter.

The effect of noncondensables on condensation is accounted for by applying a condensation suppression factor. A modified form of the correlation for condensation suppression, originally developed by Young and Bajorek

[3] has been implemented. Young and Bajorek developed a balance equation on a vapor layer which accumulates at the gas/liquid interface given by:

$$\frac{p_{dp,0} - p_{dp,i}}{p_t} = \frac{\epsilon_g}{1-\epsilon_g}\left[\frac{h_{il}\left(T_{dp,i} - T_l\right)}{\rho_g \hbar_{fg}}\right]^2 \frac{t^*}{d_{vg}} \tag{4}$$

where $p_{dp,0}$ is the bulk steam partial pressure, $p_{dp,i}$ is the steam partial pressure at the gas/liquid interface, $p_t$ is the total pressure, $\epsilon_g$ is the noncondensable gas fraction, $h_{il}$ is the liquid side heat transfer coefficient, $T_{dp,i}$ is the dew point temperature at the gas/liquid interface, $T_l$ is the liquid temperature, $\rho_g$ is the bulk vapor density, $\hbar_{fg}$ is the latent heat of vaporization, $d_{vg}$ is the diffusion constant for vapor in the noncondensable gas, and $t^*$ is the renewal time. The condensation suppression factor is determined by iteratively solving Equation (4) for the dew point temperature at the interface, $T_{dp,i}$, and then applying the definition of the suppression factor, given as the ratio of the condensation heat transfer rates with noncondensables present to that which would be calculated in pure steam :

$$x_{cond} = \frac{q_{il,NC}}{q_{il,steam}} = \frac{h_{il}\left(T_{dp,i} - T_l\right)}{h_{il}\left(T_{sat} - T_l\right)} = \frac{T_{dp,i} - T_l}{T_{sat} - T_l} \tag{5}$$

The renewal time is defined as the interval over which the gas layer can accumulate before turbulence in the vapor can sweep it away and renew the interface. An estimate for the renewal time for a jet is provided by Young and Bajorek as:

$$t^* \cong 0.01\frac{D_{jet}}{U_r} \tag{6}$$

where $U_r$ is the relative velocity between the jet and gas, which is assumed to be equal to the local jet velocity. Data from the Fundamental Condensation [1] are used to develop a correlation for the renewal time, $t^*$, consistent with the Young and Bajorek method, to account for pressure effects observed in the data but not captured by the existing correlation. The new correlation, which is solved for every point in the subgrid, is given as:

$$t^* = t_n^* \, 4.1\text{x}10^{-3}\left(\frac{\rho_l}{\rho_{g,mix}}\right)^{0.68}\left(\frac{\mu_l}{\mu_{g,mix}}\right)^{1.7}\left(\frac{p_{dp,0}}{p_T}\right)^{2.2} \tag{7}$$

where $t_n^*$ is the renewal time from Young and Bajorek, $\mu_f$ is the liquid viscosity, $\rho_{g,mix}$ is density for the steam and noncondensable mixture, $\mu_{g,mix}$ is viscosity for the steam and noncondensable mixture given in Equation (8), $p_{dp,0}$ is the steam partial pressure, and $p_T$ is the total pressure.

$$\mu_{g,mix} = \frac{p_{gas}}{p_t}\,\mu_{gas} + \frac{p_{dp,0}}{p_t}\,\mu_v \tag{8}$$

Jet breakup is modeled by calculating a critical breakup length as the minimum of the turbulent column and turbulent bag/shear breakup length correlations provided by Sallam et al [4] given as:

$$\left(\frac{L}{D}\right)_{crit} = min\begin{cases} 2.1\ We_{jet}^{0.5} \\ 11.0\ \left(\frac{\rho_l}{\rho_g}\right)^{0.5} \end{cases} \tag{9}$$

The jet Weber Number and density ratio used in the determination of the critical breakup length are calculated using conditions at the jet inlet to be consistent with correlations. The impact of jet breakup is considered by altering the interfacial area available for heat and mass transfer in the jet model. The default treatment is to assume that the jet breaks up into drops with drop diameters equal to the jet diameter, effectively increasing the interfacial area by fifty percent. Alternatively the user can specify either a drop diameter or a critical Weber Number that can be used to calculate the drop size using the local jet conditions. The interfacial area of an unbroken jet is determined from the surface area of an assumed right circular cylinder as:

$$A_{i,unbroken} = \pi D_{jet} \Delta z \tag{10}$$

where $D_{jet}$ is the local jet diameter and $\Delta z$ is the sub-grid control volume length. The broken jet interfacial area is calculated as:

$$A_{i,broken} = \frac{3}{2}\pi \frac{D_{jet}^2}{D_{drop}}\ \Delta z \tag{11}$$

The drop diameter, $D_{drop}$, is determined as described in the previous paragraph. The impact of jet breakup is ramped on between 90 and 110% of the critical breakup length to diameter ratio, so that the effective jet interfacial area is calculated as:

$$A_{i,jet} = \left(1 - \omega_{breakup}\right) A_{i,unbroken} + \omega_{breakup}\ A_{i,broken} \tag{12}$$

The ramping function is given as:

$$\omega_{breakup} = min\begin{cases} 1.0 \\ max\begin{cases} 0.0 \\ \dfrac{\left(\frac{L}{D}\right)_{jet} - 0.9\ \left(\frac{L}{D}\right)_{crit}}{0.2\ \left(\frac{L}{D}\right)_{crit}} \end{cases} \end{cases} \tag{13}$$

A low Reynolds Number jet heat transfer coefficient correction factor was developed from comparisons to jet condensation data by Celata et al [5], which showed evidence of enhanced heat transfer with decreasing Reynolds Number. The correction factor is implemented as a multiplier, $\omega_{Re}$, on the jet Stanton Number given in Equation (1), which takes the form:

$$\omega_{Re_{low}} = max\begin{cases} 1.0 \\ \dfrac{5000.0}{Re_{jet}} \end{cases} \tag{14}$$

The jet Reynolds Number is calculated using the diameter for the length scale and using local conditions.

The effect of a jet path crossing through a COBRA-IE control volume filling with liquid is accounted for a liquid filling multiplier. When a jet path passes into, or through, a liquid filled COBRA-IE control volume, the heat transfer coefficient is ramped to zero in the current, and all, subsequent, sub-grid control volumes as a cubic function of the COBRA-IE gas volume fraction as:

$$\omega_{liqfill} = \left(3.0\ \omega_{\alpha_g} - 2.0\ \omega_{\alpha_g}\right)\ \omega_{\alpha_g}^2 \tag{15}$$

The void fraction multiplier, $\omega_{\alpha_g}$, is given as:

$$\omega_{\alpha_g} = min\begin{cases}1.0\\ max\begin{cases}0.0\\ \dfrac{\alpha_g - \alpha_B}{\alpha_{SA} - \alpha_B}\end{cases}\end{cases} \tag{16}$$

The upper and lower bounds of the interpolation, $\alpha_{SA}$ and $\alpha_B$, are the upper and lower bounds of the large bubble flow regime in COBRA-IE, which are 0.5 and 0.2 respectively. The jet condensation heat transfer coefficient is calculated as:

$$h_{jet} = St_{jet} Pr_l Re_{jet} \frac{k_l}{D_{jet}} \omega_{Re_{low}} \omega_{liqfil} \tag{17}$$

The jet Stanton Number is calculated using local conditions in Equation (1), the liquid Prandtl and Reynolds Numbers as well as the liquid thermal conductivity are calculated using local conditions and the low Reynolds Number and liquid filling multipliers are calculated as given in Equations (14) and (15).

## 4. JET BOUNDARY CONDITION SOLUTION

### 4.1. Marching Solution

The user supplied jet trajectory is internally discretized to ensure that each sub-grid control volume exists entirely within a single COBRA-IE control volume. A sensitivity study was performed in the development of the solution method to demonstrate that a node size of 1.27 cm (0.5 in) provides sufficient accuracy. As such, the node size is automatically selected to be as close to 1.27 cm without being larger.

For each time step the jet path initial conditions are determined from the user supplied head flow curve, boundary condition fluid conditions, and path flow split information. Given the initial conditions, the jet conservation equations are then solved for each sub-grid control volume. The inlet conditions for each control volume are the mass flow rate, enthalpy, density, local jet diameter, and local jet length. The jet specific closure relations are calculated using local conditions as described in the previous section. The average jet diameter, over the length of the jet from point of injection, is used to determine the jet length to diameter ratio used in the closure relations. Conditions in the COBRA-IE control volume are used to determine the saturation properties, the steam and noncondensable gas partial pressures, densities, and gas mixture viscosity. The interfacial area is given from Equation (11).

Once the jet condensation heat transfer coefficient, $h_{jet}$, condensation suppression factor, $x_{cond}$, and interfacial area, $A_{i,jet}$, have been determined, the interfacial heat transfer rate can be calculated as:

$$q_{il} = h_{jet} x_{cond} A_{i,jet} \frac{\hbar_{l,sat} - \hbar_l}{c_p} \tag{18}$$

where $\hbar_{l,sat}$ is the saturated liquid enthalpy. The rate of phase change in the sub-grid control volume can then be calculated as:

$$\Gamma = -\frac{q_{il}}{\hbar_v - \hbar_{l,sat}} \tag{19}$$

Once the condensation rate is determined the mass flow rate out of the jet sub-grid control volume is determined from the steady-state conservation of mass as:

$$\dot{m}_{\text{out}} = \dot{m}_{\text{in}} - \Gamma \tag{20}$$

The jet enthalpy at the control volume exit is determined from the steady-state conservation of thermal energy as:

$$\hbar_{out} = \frac{\dot{m}_{in}\hbar_l - \Gamma\hbar_{l,sat} + q_{il}}{\dot{m}_{out}} \tag{21}$$

The condensation heat transfer rate is limited such that the jet enthalpy at the exit of the sub-grid control volume cannot be greater than the saturated liquid enthalpy. The jet diameter at the exit of the control volume is calculated by assuming that the jet is not accelerated by the addition of the condensate (and neglecting the potential effects of gravity since the jet path orientation is not specified) and accounting for all changes in mass flow rate to either changes in density or changes in flow area. The jet diameter at the control volume exit is:

$$D_{jet,out} = \sqrt{\frac{4.0\ \dot{m}_{out}}{\pi\ \rho_{l,out}\ U_{jet}}} \tag{22}$$

where $\rho_{l,out}$ is the liquid density calculated using the jet exit enthalpy and $U_{jet}$ is the inlet jet velocity. The sub-grid control volume exit quantities are then used at the inlet quantities for the next sub-grid control volume. This is repeated in a marching solution until the end of the jet path is reached.

The condensation rate and the vapor energy associated with the jet condensation (product of condensation rate and vapor enthalpy in the COBRA-IE control volume) are summed over all of the sub-grid control volumes within a COBRA-IE control volume and stored for use in the boundary condition interface calculations described in the next sub-section. For the last sub-grid control volume in the jet path; the jet exit mass flow rate, liquid energy rate (product of mass flow rate and exit enthalpy), and exit density are stored for use in interface calculations.

## 4.2. Interface with COBRA-IE

The jet injection boundary condition interfaces with COBRA-IE through a series of function calls that account for the impact of condensation along the length of the jet paths and the deposition of the liquid at the jet ends. During boundary condition input processing tallies are made to determine the number of jet paths or ends that pass through or exist in any COBRA-IE control volume. The jet boundary condition, path and control volume and end numbers that reside in a control volume are also stored at this time.

If the number of paths which pass through a COBRA-IE control volume is greater than zero, two function calls are made to calculate the total mass transfer rate of vapor which is removed from the control volume as well as the total energy transfer rate associated with the vapor mass removed. These two quantities are included, as explicit terms, in the vapor mass and energy conservation equations solved by COBRA-IE.

If the number of jet path ends in a COBRA-IE control volume is greater than zero, a total of four function calls are made. Two functions are used to calculate the total rate at which mass of continuous liquid and entrained

liquid mass is deposited in the control volume. The third function returns the calculated rate at which liquid energy is added to the control volume due to the combined entrained and continuous liquid mass transfer rates. This is because, while COBRA-IE solved a three-field representation of the two-fluid system, a single liquid energy equation is solved. These three calculated quantities are included, as explicit terms, in the entrained liquid mass, continuous liquid mass, and total liquid energy equations. The final function call calculates the rate at which droplet interfacial area is added to the cell for inclusion the drop interfacial area transport equation solved by COBRA-IE.

The calculations described in the previous two paragraphs utilize user input for:

(a) The number of actual jets each path represents, $N_{jet,path}$. This is used as a multiplier on the vapor mass and energy transfer rates for that particular path. It is also used as a multiplier on the entrained and continuous liquid mass transfer rates, the total liquid energy transfer rate, and the droplet interfacial area production rate.
(b) The end fraction, $\epsilon_{end}$. This represents the fraction of the path that is deposited at this end. It is used as a multiplier on the entrained and continuous liquid mass transfer rates, the total liquid energy transfer rate, and the droplet interfacial area production rate.
(c) The end drop fraction, $\epsilon_{d,end}$. This is used to split the liquid flow rate in a jet path end between the entrained liquid and continuous liquid fields.
(d) The end drop size, $D_{d,end}$. This is used to calculate the drop interfacial area production rate bases on the jet end entrained liquid mass transfer rate.

The formulation for the vapor mass transfer rate source, $\mathcal{S}m_{v_{I,J}}$, in a given COBRA-IE control volume is given by performing a summation over all of the path nodes which pass through the cell as:

$$\mathcal{S}m_{v_{I,J}} = \sum_{nn=1}^{N_{nodes_{IJ}}} \Gamma_{nn} N_{jet,path} \tag{23}$$

where $\Gamma_{nn}$ is the condensation rate in the path node, $N_{jet,path}$ is the number of actual jets represented by the path, and $N_{nodes_{I,J}}$ is the number of sub-grid nodes in Channel $I$, Volume $J$.

When calculating the mass and energy source terms associated with Channel $I$, Volume $J$, the source terms for all of the paths or ends that interact with that volume are summed. The formulation for the vapor energy transfer rate in a given COBRA-IE cell follows as:

$$\mathcal{S}e_{v_{I,J}} = \sum_{nn=1}^{N_{nodes_{I,J}}} \Gamma_{nn} \hbar_{v,nn} N_{jet,path} \tag{24}$$

where $\hbar_{v,nn}$ is the vapor enthalpy in the COBRA-IE cell association with the path node and $N_{nodes_{I,J}}$ is the number of sub-grid nodes in Channel $I$, Volume $J$.

The formulation for entrained liquid mass transfer rate in a given COBRA-IE cell is given by performing a summation over all of the path ends in the cell as:

$$\mathcal{S}m_{e_{I,J}} = \sum_{ee=1}^{N_{ends_{I,J}}} \dot{m}_{path} N_{jet,path} \epsilon_{end,ee}\, \epsilon_{d,ee} \tag{25}$$

where $\dot{m}_{path}$ is the mass flow rate at the end of the path associated with the jet end, $N_{jet,path}$ is the number of actual jets represented by the path, $\epsilon_{end,ee}$ is the end fraction, $\epsilon_{d,ee}$is the end drop fraction, and $N_{ends_{I,J}}$ is the number of path ends in Channel $I$, Volume $J$.

The formulation for the continuous liquid mass transfer rate in a given COBRA-IE cell is given as:

$$\mathcal{S}m_{l_{I,J}} = \sum_{ee=1}^{N_{ends_{I,J}}} \dot{m}_{path} N_{jet,path} \epsilon_{end,ee} \left(1 - \epsilon_{d,ee}\right) \tag{26}$$

where $\dot{m}_{path}$ is the mass flow rate at the end of the path associated with the jet end, $N_{jet,path}$ is the number of actual jets represented by the path, $\epsilon_{end,ee}$ is the end fraction, $\epsilon_{d,ee}$is the end drop fraction, and $N_{ends_{I,J}}$ is the number of path ends in Channel $I$, Volume $J$.

The formulation for the total liquid energy transfer rate in a given COBRA-IE cell is given as:

$$\mathcal{S}e_{l_{I,J}} = \sum_{ee=1}^{N_{ends_{I,J}}} \dot{m}_{path} \hbar_{l,ee} N_{jet,path} \epsilon_{ee} \tag{27}$$

where $\dot{m}_{path}$ is the mass flow rate at the end of the path associated with the jet end, $\hbar_{l,ee}$ is the liquid enthalpy in the COBRA-IE cell association with the path node, $N_{jet,path}$ is the number of actual jets represented by the path, $\epsilon_{d,ee}$is the end drop fraction, and $N_{ends_{I,J}}$ is the number of path ends in Channel $I$, Volume $J$.

The formulation for the drop interfacial area production rate in a given COBRA-IE cell is given as:

$$\mathcal{S}A_{i,jet_{I,J}} = \sum_{ee=1}^{N_{ends_{I,J}}} \frac{6.0\, \dot{m}_{path} N_{jet,path} \epsilon_{end,ee} \epsilon_{d,ee}}{D_{d,ee}\, \rho_l} \tag{28}$$

## 5. SELECTED RESULTS

The sub-grid jet model, including the constitutive relationships, has been assessed against Fundamental Condensation Test data [1] for situations with and without non-condensables present. This data set covers a wide range of nominal conditions including: pressures from near atmospheric to 1.7 $MPa$, non-condensable gas volume fractions up to 0.5, jet diameters of 2.54 and 5.08 $mm$, liquid injection temperatures between 300 and 340 $K$, and flow rates from 1.9 to 30 $L/m$ resulting in jet velocities between 6 and 50 $m/s$. The test was designed such that temperature measurements could be taken along the length of the jet, up to 1.2 $m$.

The ability of the sub-grid jet model to predict the enthalpy rise along the length of a condensing jet in both pure steam and with a non-condensable gas present is shown in Figure 2. From the figure, it can be concluded that the sub-grid model as a whole, including the implementation of the jet specific closure relationships, is able to accurately predict condensation heat transfer on a liquid jet, both in pure steam and in the presence of a non-condensable gas.

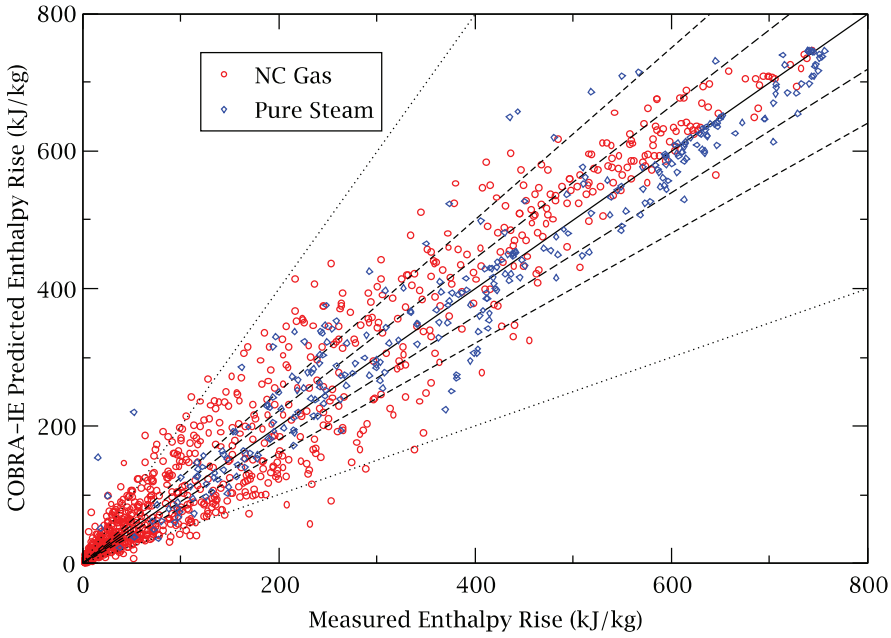


**Figure 2: Predicted vs. Measured Jet Enthalpy Rise**

The data shown in Figure 2 can be used to compare the code average heat transfer coefficient to an average heat transfer coefficient from the data using the following formulation:

$$\bar{h}_{jet} = \frac{\dot{m}_{jet}\left(\hbar_{jet} - \hbar_{jet,in}\right)}{A_{i,jet}\Delta\hbar_{log}} \tag{29}$$

The log mean enthalpy difference is:

$$\Delta\hbar_{log} = \frac{\hbar_{jet} - \hbar_{jet,in}}{log\left(\frac{\hbar_{l,sat} - \hbar_{jet,in}}{\hbar_{l,sat} - \hbar_{jet}}\right)} \tag{30}$$

In the previous two equations, the jet mass flow rate, $\dot{m}_{jet}$, jet inlet enthalpy, $\hbar_{jet,in}$, and jet interfacial area, $A_{i,jet}$, are the same for both the COBRA-IE simulation and the data. A ratio of the measured to predicted heat transfer coefficients can be simplified to:

$$\left(\frac{M}{P}\right)_{h_{jet}} = \frac{log\left(\frac{\hbar_{l,sat} - \hbar_{jet,in}}{\hbar_{l,sat} - \hbar_{jet,data}}\right)}{log\left(\frac{\hbar_{l,sat} - \hbar_{jet,in}}{\hbar_{l,sat} - \hbar_{jet,COBRA}}\right)} \tag{1}$$

A histogram of the measured to predicted jet heat transfer coefficients, using the data in Figure 2 for cases in pure steam only, is shown in Figure 3. Similarly, the histogram of the measured to predicted effective jet heat transfer coefficients, including the condensation suppression factor, with noncondensable gas present is given in Figure 4.

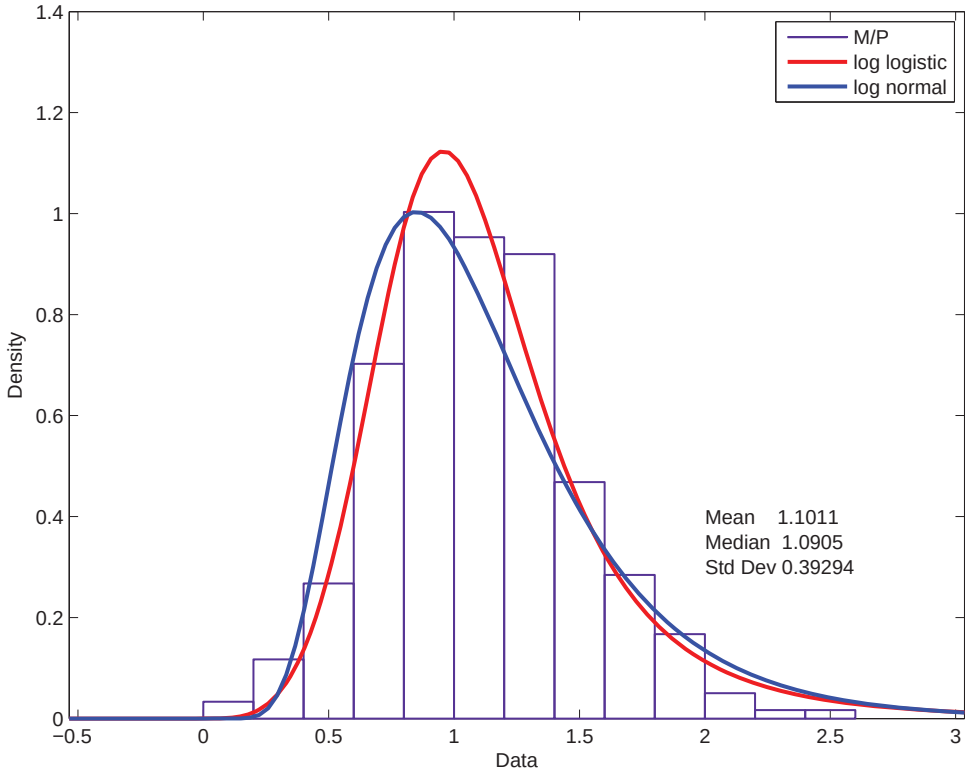


**Figure 3: Ratio of Measured to Predicted Jet Condensation Heat Transfer Coefficient for Pure Steam**

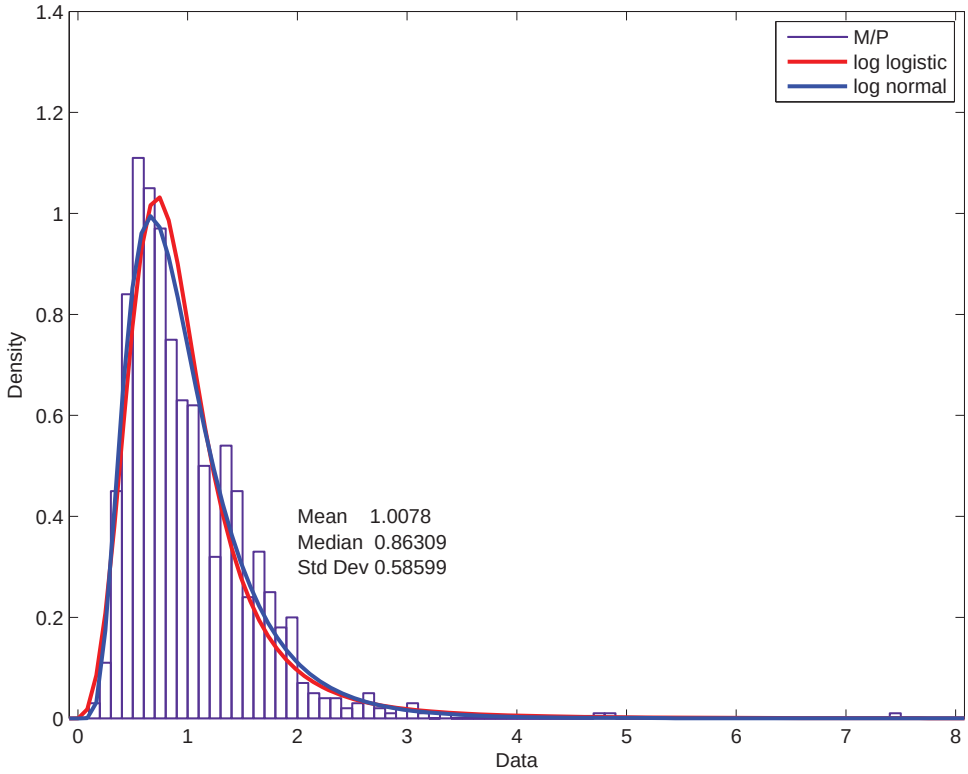


**Figure 4: Ratio of Measured to Predicted Jet Condensation Effective Heat Transfer Coefficient with Noncondensable Gas Present**

The next two figures show examples of the capability of the sub-grid jet model to predict the jet enthalpy along the jet length for a case in pure steam and a case with fifty percent noncondensable gas by volume and compare those results with an attempt to model the facility without the benefit of the jet injection boundary condition. Both of these cases were run at 344 kPa (50 psi), with an injection temperature of 300 K (80 $^{o}$F), and a jet flow rate of 7.5 L/min (2 gpm). These figures demonstrate that the jet injection boundary condition is able to predict well, not only the average condensation heat transfer rates, but also the local jet heat transfer characteristics. Figure 5 also demonstrates the deficiency in the base COBRA-IE representation in modeling jets. By depositing all of the continuous liquid as a thin film, the interfacial area, and therefore the condensation rates are overestimated. Almost the entirety of the condensation potential is realized in the first control volume. The base COBRA-IE representation, even when the condensation rate is severely limited by the presence of noncondensables, over predicts the condensation rate in the injection control volume.

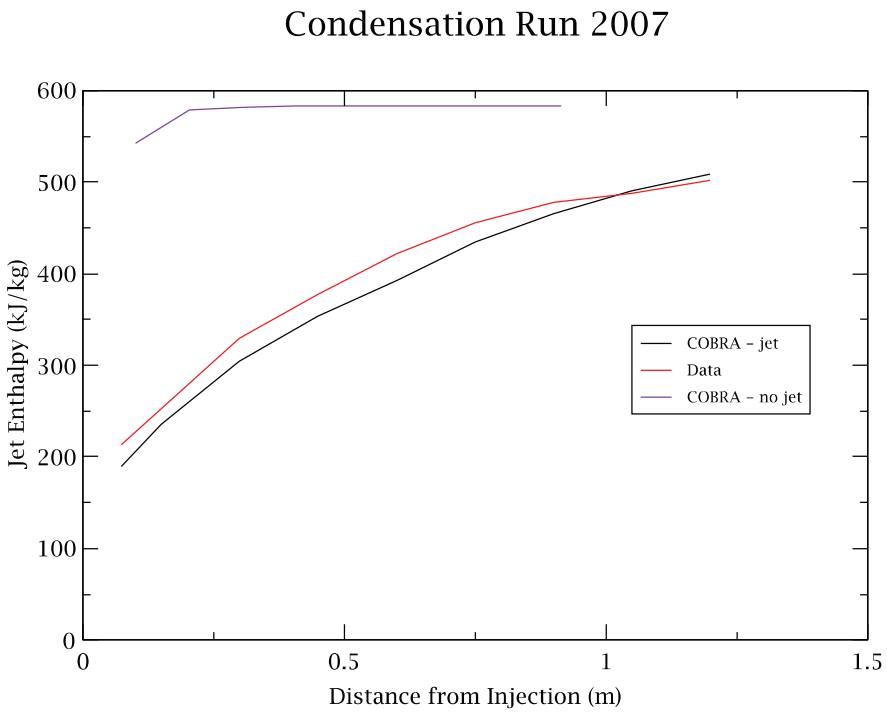


**Figure 5: Jet Enthalpy as a Function of Jet Length in Pure Steam**

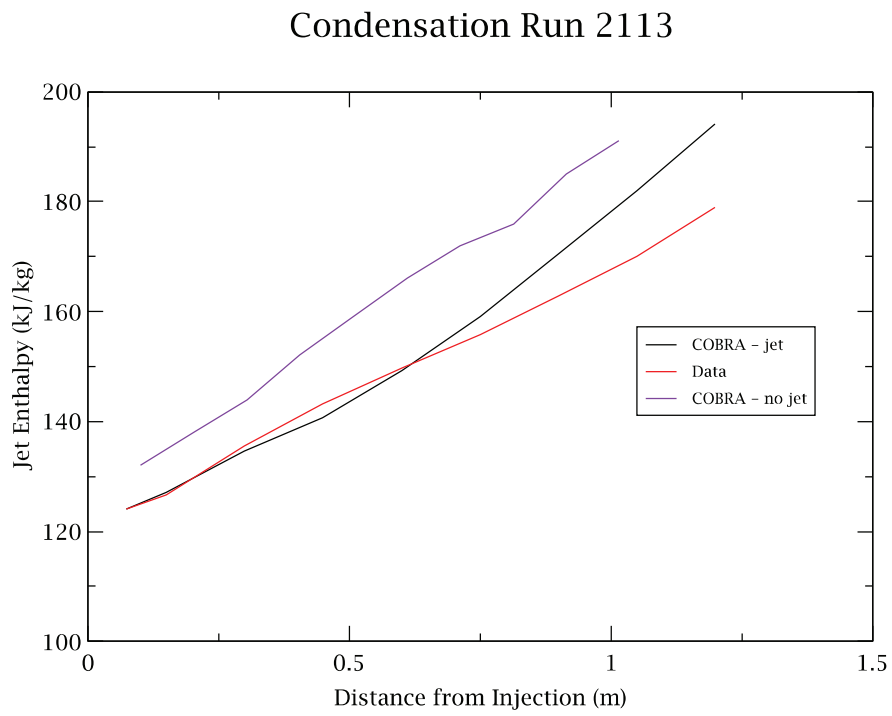


**Figure 6: Jet Enthalpy as a Function of Jet Length with 50% Noncondensable gas Volume Fraction**

## 6. CONCLUSIONS

A jet injection boundary condition, which employs a sub-grid jet condensation model, has been developed for COBRA-IE. The sub-grid jet condensation model allows for provides a more detailed estimate of the condensation rate on the jet within the COBRA–IE node and allows the use of jet specific closure relationships related to condensation heat transfer. The jet injection boundary condition has been implemented in a way to maximize the flexibility to the user to model situations in which condensation on liquid jets may be important. The implementation of the boundary condition and the jet condensation closure models have been assessed against fundamental direct contact condensation data both in pure steam and in the presence of noncondensable gas. The results of these comparisons show that the model in its entirety is able to predict both the average jet heat transfer rates over the length of the jet and the heat transfer rates on a local basis.

## NOMENCLATURE

| | |
|---|---|
| $-\Gamma$ | Condensation rate |
| $\dot{m}$ | Mass flow rate |
| $\hbar$ | Enthalpy |
| $\hbar_{l,sat}$ | Saturated liquid enthalpy |
| $\hbar_{fg}$ | Latent heat of vaporization |
| $p$ | Pressure |
| $p_{dp}$ | Dew point pressure |
| $T$ | Temperature |
| $T_l$ | Liquid temperature |
| $T_{sat}$ | Saturation temperature |
| $\Delta h_{log}$ | Log mean enthalpy difference |
| $c_p$ | Specific heat |
| $T_{dp}$ | Dew point temperature |

| | |
|---|---|
| $h_{il}$ | Liquid side heat transfer coefficient |
| $A_i$ | Interfacial area |
| $L$ | Jet length |
| $D_{jet}$ | Jet diameter |
| $k_l$ | Liquid thermal conductivity |
| $St$ | Stanton Number |
| $Re$ | Reynolds Number |
| $Pr$ | Prandtl Number |
| $We$ | Weber Number |
| $\rho_l$ | Liquid density |
| $\rho_v$ | Vapor density |
| $\rho_g$ | Gas mixture density |
| $x_{cond}$ | Condensation suppression factor |
| $\mu_f$ | Liquid viscosity |
| $\mu_{g,mix}$ | Gas mixture viscosity |
| $\epsilon_g$ | Noncondensable gas volume fraction |
| $t^*$ | Renewal time |
| $f_{t^*}$ | Renewal time multiplier |
| $U_{jet}$ | Jet velocity |
| $d_{vg}$ | Mass diffusion coefficient of steam in gas |
| $q_{il}$ | Liquid side interfacial heat transfer rate |
| $\omega$ | Multiplier on Stanton Number |
| $\mathcal{S}m$ | Source term in mass conservation equation |
| $\mathcal{S}e$ | Source term in energy conservation equation |
| $\mathcal{S}A_i$ | Source term in drop interfacial area equation |

## REFERENCES


1. F. X. Buschman, et al., "Fundamental Experiments of Condensation Heat Transfer on Water Jets in the Presence of Noncondensable Gas", *NURETH-16*, Chicago, August 30 – September 4 (2015).
2. F. X. Buschman, "Development of a Liquid Jet Model for Implementation in a 3-Dimensional Eularian Analysis Tool", Ph. D. Dissertation in Nuclear Engineering, Department of Mechanical and Nuclear Engineering, The Pennsylvania State University (2008).
3. M. Y. Young and S.M. Bajorek, "The Effect of Noncondensables on Condensation in Reactor LOCA Transients", *AICHE Heat Transfer Conference*, Baltimore (1997).
4. K. Sallam, A. Dai, G. Faeth, "Liquid Breakup at the Surface of Turbulent Round Liquid Jets in Still Gases", *International Journal of Multiphase Flow*, **28**, pp. 427-449 (2002).
5. G.P. Celata, M. Cumo, G.E. Farello, and G. Focardi, "A Comprehensive Analysis of Direct Contact Condensation of Saturated Steam on Subcooled Liquid Jets", *International Journal of Heat Mass Transfer*, **32**(4), pp. 639-654 (1989).